Development 130, 3567-3578

doi:10.1242/dev.00581

DEVELOPMENT AND DISEASE

The role of chordin/Bmp signals in mammalian pharyngeal development and DiGeorge syndrome

Daniel Bachiller[1,2,*,†], John Klingensmith[3,4,*], Natalya Shneyder[2], Uyen Tran[1], Ryan Anderson[3], Janet Rossant[4] and E. M. De Robertis[1]

[1]Howard Hughes Medical Institute and Department of Biological Chemistry, University of California, Los Angeles, CA 90095-1662, USA
[2]Victor Goodhill Ear Center, Head and Neck Surgery Division, University of California, Los Angeles, CA 90095-1794, USA
[3]Department of Cell Biology, Duke University Medical Center, Durham, NC 272710, USA
[4]Samuel Lunenfeld Research Institute, Mount Sinai Hospital, University of Toronto, Toronto, M5G 1X5, Canada
*These authors contributed equally to this work
[†]Author for correspondence (e-mail: bachiller@hnsurg.medsch.ucla.edu)

Accepted 24 April 2003

SUMMARY

The chordin/Bmp system provides one of the best examples of extracellular signaling regulation in animal development. We present the phenotype produced by the targeted inactivation of the chordin gene in mouse. Chordin homozygous mutant mice show, at low penetrance, early lethality and a ventralized gastrulation phenotype. The mutant embryos that survive die perinatally, displaying an extensive array of malformations that encompass most features of DiGeorge and Velo-Cardio-Facial syndromes in humans. Chordin secreted by the mesendoderm is required for the correct expression of *Tbx1* and other transcription factors involved in the development of the pharyngeal region. The chordin mutation provides a mouse model for head and neck congenital malformations that frequently occur in humans and suggests that chordin/Bmp signaling may participate in their pathogenesis.

Key words: Chordin, Bmp, Tbx1, Fgf8, DiGeorge, Pharyngeal endoderm, Ventralization, Neural crest, Patterning, Persistent truncus arteriosus, Mouse

INTRODUCTION

Dorsoventral patterning in vertebrates and invertebrates is regulated by a positional information gradient established by the opposing activities of bone morphogenetic proteins (Bmps) and the antagonists chordin (Chrd)/short gastrulation (Sog) (De Robertis and Sasai, 1996; Francois et al., 1994; Sasai et al., 1994). In *Drosophila* early development, Sog is expressed ventrally and regulates the activity of the dorsally expressed Decapentaplegic (Dpp) (Francois et al., 1994). In vertebrates, the Bmp/Chrd regulatory pathway of extracellular signals is linked to the activity of dorsal organizer centres (Bachiller et al., 2000; De Robertis et al., 2000). In zebrafish, genetic analyses have shown that inhibition of Bmp signaling by Chrd is required for the correct development of the neural plate and dorsal mesoderm (Schulte-Merker et al., 1997). In *Xenopus*, knockdown of *Chrd* expression using specific morpholino oligonucleotides causes reduction of neural plate and expansion of ventral mesoderm (Oelgeschlager et al., 2003). In experimental *Xenopus* embryonic assays, *Chrd* is required for dorsalization by lithium chloride or activin treatments, and for neural induction by Spemann organizer grafts (Oelgeschlager et al., 2003).

We report the loss-of-function mutation in the murine *Chrd* gene. At day 8.5 of gestation (E8.5), a small fraction of homozygous mutant embryos displayed a ventralized phenotype in which the allantois was expanded and the embryonic region reduced in size. At gastrula and neurula stages *Chrd* is expressed in the endomesoderm of the midline and in Hensen's node. Loss of homozygotes was observed also at late gestation, but some *Chrd* mutants survived and died of cardio-respiratory failure at birth. These mutants closely mimic the alterations recently described for *Tbx1* homozygous mouse mutants (Jerome and Papaioannou, 2001; Lindsay et al., 2001; Merscher et al., 2001; Vitelli et al., 2002a) and recapitulate the pharyngeal malformations characteristic of DiGeorge/Velo-Cardio-Facial (DGS/VCFS) syndromes (Ryan et al., 1997) in humans. At mid embryogenesis, mouse *Chrd* is expressed in the endoderm of the pharynx.

DGS/VCFS is the most common chromosomal microdeletion syndrome in humans, affecting 1 in 4000 live births (Wilson et al., 1994). DGS/VCFS is predominantly

associated with haploinsufficient microdeletions in human chromosome 22q11. DiGeorge syndrome was initially identified in cases of isolated T cell immunodeficiency (DiGeorge, 1968; Gatti et al., 1972; Harington, 1828-1829), but currently the term covers a spectrum of head and neck malformations, including hypoplasia of thymus and parathyroid and thyroid glands, cleft palate, facial dysmorphism with low setting of the external ear, small jaw, deafness, and cardiac defects. The congenital heart malformations arise from incomplete septation of the outflow tract (a defect frequently associated with defective migration of the neural crest into the developing heart), and constitute the primary cause of death in affected individuals (Ryan et al., 1997).

The defects observed in individuals with DGS/VCFS involve organs and structures originating from the pharyngeal endoderm or adjacent tissues during embryogenesis. Similar DiGeorge-like pharyngeal malformations are seen in acquired syndromes caused by retinoic acid, alcohol or other in utero teratogens (Ammann et al., 1982; Lammer et al., 1985; Oster et al., 1983). *Chrd* mutant neonates display phenotypes characteristic of DiGeorge syndrome: lack of thymus and parathyroid glands, lack of heart colonization by neural crest, defects in pharyngeal arches 2-6, cleft palate and abnormal placement of the external ear. Two different developmental mechanisms have been proposed as possible explanations for the pathogenesis of DiGeorge syndrome: incomplete differentiation of the pharyngeal pouches (Wendling et al., 2000) and inability of peripharyngeal neural crest cells to migrate to their target organs (Kirby and Bockman, 1984). Both processes are affected in *Chrd* homozygous mouse mutants.

MATERIALS AND METHODS

Generation of *Chrd^{tm1DR}* mice

The targeting construct included stop codons in the three possible reading frames inserted in a unique *Sfi*I site. For genotyping purposes the *Sfi*I site was replaced by an *Eco*RV site (Fig. 1G). The presence of the IRES-*lacZ* and neo^r cassettes introduces a frameshift immediately after CR1. The construct with the mutant allele was electroporated into R1 embryonic stem (ES) cells (Nagy et al., 1993), and homologous recombination in the *Chrd* locus detected by Southern (Fig. 1H) and PCR (Fig. 1I) analysis. The primers used were: Chrd-F1 (5′-GGTGGGCCTGATGAAGTTTGAGTC-3′), Chrd-R1 (5′-CCTACACATCCCCACCTCTCTAAA-3′) and Neo-2 (5′-GTTCCACATACACTTCATTCTCAG-3′). The PCR reactions yield bands of 2.87 and 2.78 kb for mutant and wild-type alleles, respectively. The *lacZ* reporter was not active because of a mutation in the internal ribosomal entry site (IRES) in the construct. The original 129Sv/J heterozygous males obtained from mating the founding chimeras were crossed with hybrid B6SJLF1 females (Jackson laboratories), and the resulting heterozygous males subsequently backcrossed with B6SJLF1 females for 10 additional generations. The phenotype of *Chrd*$^{-/-}$ animals in the inbred 129Sv/J and the mixed B6SJLF1 line was as described here, but in the F1 product of the cross 129Sv/J inbred×ICR outbred (Harlan) homozygous mutants showed a milder phenotype and were viable and fertile. The same phenotypes were observed in mice derived from two independently targeted cell lines. Mice for analysis were obtained by crossing heterozygous parents of B6SJLF1 background.

Embryo genotyping

DNA was extracted from extra-embryonic membranes of E8.5 embryos or older, and from tails of newborns. The tissues were digested at 55°C overnight in 50 mM Tris-HCl pH 8, 100 mM EDTA, 100 mM NaCl, 1% SDS and 0.5 mg ml^{-1} Proteinase K. After adding NaCl to 1 M final concentration, the mix was centrifuged for 15 minutes, the supernatant recovered and DNA precipitated with an equal volume of isopropanol. Genotypes were determined by PCR using a mix of the three following primers: Chrd-F2 (5′-GAGTTAGGAGGTGGAGCTCTTACAC-3′), Chrd-R2 (5′-GGTAGGAGACAGAGAAGCGTAAACT-3′) and the same Neo2 primer used in the ES cell genotyping. They yielded bands of 416 and 282 bp for the wild-type and the mutant allele, respectively (Fig. 1I).

In situ hybridization, histological and skeletal preparations

Whole-mount in situ hybridization was performed as described (Bachiller et al., 2000) (http://www.hhmi.ucla.edu/derobertis/index.html). Newborn and 14.5-day-old mouse embryos were fixed in Bouin's solution, dehydrated, cleared and embedded in paraffin wax. Serial sections (8 μm) were stained according to the Mallory's Tetrachrome method or with Eosin/Hematoxylin. For sections shown in Fig. 8, embryos were fixed in paraformaldehyde for 4 hours after in situ hybridization, dehydrated, embedded in Ducupan (Fluka) and sectioned at 10 μm. Alcian Blue/Alizarin Red skeletal staining was performed as described (Belo et al., 1998).

Xenopus injections and VMZ assays

RT-PCR of *Xenopus* embryos was performed as described (http://www.hhmi.ucla.edu/derobertis/). Briefly, embryos were injected with 50 pg *Chrd* mRNA in the ventral marginal side at the four-cell stage, dorsal (DMZ) and ventral marginal zones (VMZ) dissected at stage 10, cultured until sibling embryos reached stage 14 and processed for RT-PCR. *Tbx1* (Accession Number AF526274) was amplified with the following primers: upper primer (5′-CCAGGAAAAGGGAGCAAC-3′); lower primer (5′-TCGCAAAAATGGGAGAGC-3′). *Fgf8* (Accession Number AF461177) was amplified with primers that recognized all isoforms of the *Xenopus* gene: upper primer (5′-GGAGACTGGTTACTACAT-3′); lower primer (5′-ACCCCTTCTTGTGAAAG-3′).

RESULTS

Gastrulation defects in *Chrd$^{-/-}$* mice

The Chrd secreted Bmp-binding protein is expressed in the mouse node and its derivatives, notochord and pharyngeal endoderm (Fig. 1A-F). The Chrd protein contains four cysteine-rich (CR) domains, all of which are able to bind Bmps. CR1 and CR3 show the highest affinity for Bmp4, and can antagonize Bmp signals upon mRNA injection into *Xenopus* embryos (Larrain et al., 2000). To generate a null allele of *Chrd*, we prepared a targeting construct with translation stop codons in the three possible reading frames within the signal peptide region. The stop codons were followed by a frameshift and the insertion, after CR1, of IRES-*lacZ* and PGK-neo cassettes that further disrupted the *Chrd* gene (Fig. 1G). Transcripts from this *Chrd^{tm1DR}* allele (hereafter referred to as *Chrd*$^-$) were undetectable in *Chrd$^{-/-}$* embryos at the node stage (Fig. 1J, arrowhead).

Heterozygous *Chrd* mice were viable and fertile and were mated to generate *Chrd$^{-/-}$* embryos of various developmental stages. At day E8.5, we observed the presence of resorption nodules in the uterus of pregnant females and a small reduction in the expected number of *Chrd$^{-/-}$* embryos (50 recovered, 57 expected). Four genotyped homozygous mutant embryos

showed a clear reduction in the size of the embryonic region, accompanied by an enlargement of the allantois with respect to the rest of the embryo (Fig. 2A,A′). In histological sections, a considerable hypoplasia of the neural plate (Fig. 2B,B′), absence of somites and notochord (Fig. 2C,C′), and an abundance of extra-embryonic mesodermal cells in the allantois (Fig. 2D,D′) were observed. The rest of the mutants (46) were morphologically indistinguishable from their heterozygous and wild-type littermates. The phenotype of the four abnormal mutants was similar to, but less pronounced than, the ventralization of the mesoderm observed in double homozygous *Chrd*;*Nog* mutants (Bachiller et al., 2000) in which, in addition, anterior truncations of the neural plate were also present.

In zebrafish and *Xenopus*, inactivation of *Chrd* causes an expansion of ventral mesoderm and reduction of dorsal mesoderm and neural plate (Schulte-Merker et al., 1997). In mammals, the mesoderm forms during gastrulation by the ingression of epiblast cells through the primitive streak. Cells exiting at the posterior end of the primitive streak move into the extra-embryonic region where they give rise to a mesodermal lineage (allantois, amnion and blood islands of the yolk sac) equivalent to the ventral mesoderm of *Xenopus*. By contrast, cells located in more anterior regions of the streak remain inside the embryo proper and produce the paraxial,

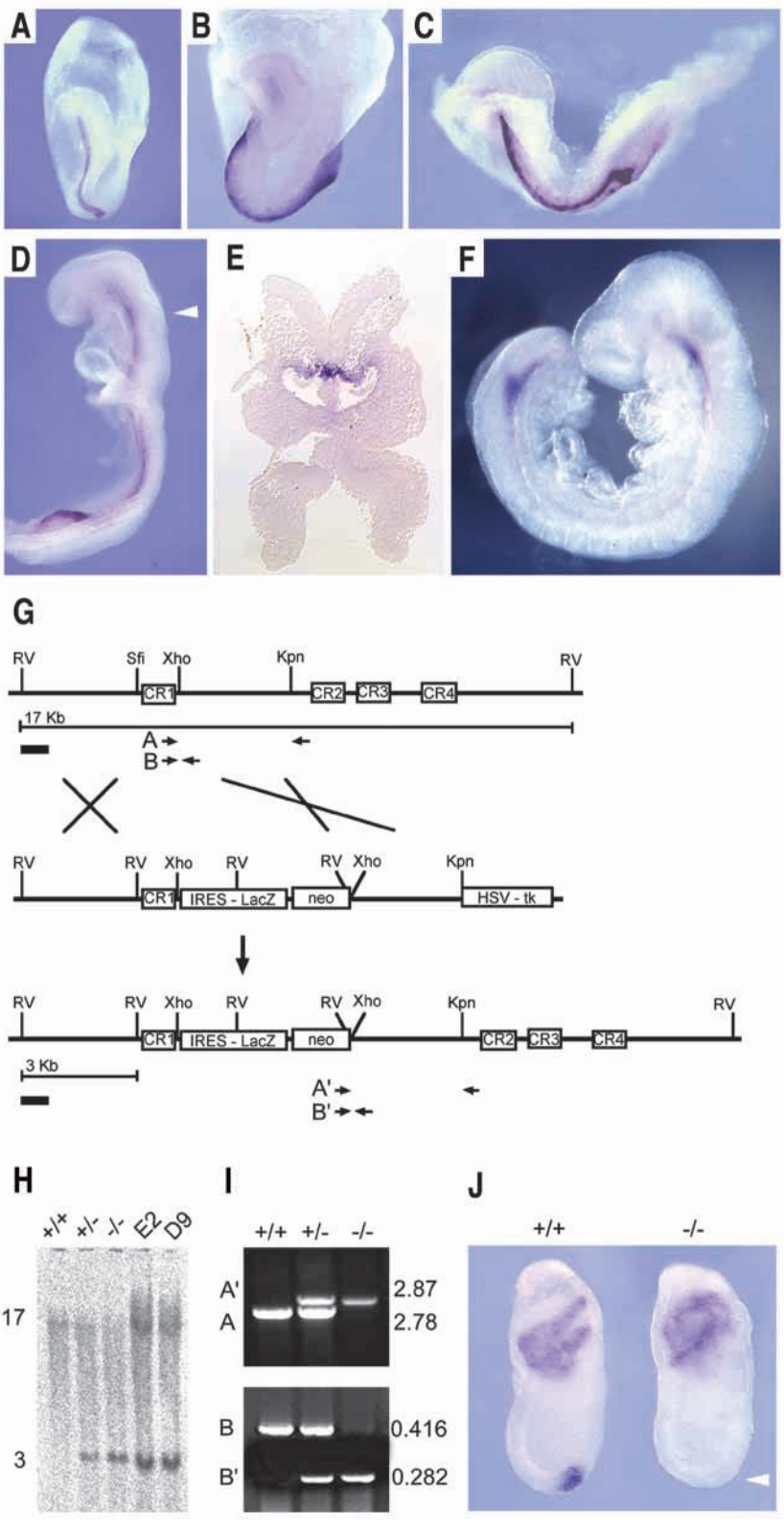

Fig. 1. Expression pattern and targeted homologous recombination of the *Chrd* gene. (A-F) Whole mount in situ hybridization with *Chrd* probe. (A) At E7, the expression domain of *Chrd* extends from the rostral limit of the notochord to the node. (B,C) As gastrulation progresses and the node moves posteriorly, *Chrd* expression in the newly formed axial mesendoderm is maintained. (D,E) After the embryo turns, *Chrd* transcripts are present in the dorsal endoderm adjacent to the notochord; the arrowhead indicates the level of the section in E. (F) By late E 8.5, the axial expression of *Chrd* has disappeared from most of the trunk and tail, but it is still strong in the pharynx, chordoneural hinge of the tailbud and postanal gut. (G) Schematic representation of the chordin locus (top), targeting construct (middle) and mutant allele (bottom). The approximate location of the four cysteine-rich repeats is indicated by boxes. The position of the primers used in the genotyping reactions (A,A′,B,B′) is indicated by arrows. The thick black bars indicate the location of the probe used to distinguish between recombination events occurring 5′ or 3′ of the stop codons placed at the *Sfi*I site. (H) Southern blot analysis of genomic DNA from two targeted cell lines (E2 and D9) and wild-type, heterozygous and homozygous mutant embryos digested with *Eco*RV. The 17 kb band corresponds to the wild type allele. The 3 kb band results from an homologous recombination event 5′ of the stop codons inserted at *Sfi*I. (I) PCR analysis of embryos obtained from matings between heterozygous mice. (A,A′) PCR amplifications used in the original ES cell screening. (B,B′) Amplifications used to genotype the animals during the study. (J) In situ hybridization analysis of *Chrd* and *Bmp4* expression in wild-type and *Chrd*$^{-/-}$ embryos. Both antisense probes were transcribed from full-length cDNA clones. The arrowhead indicates the lack of *Chrd* transcripts in the node of the mutants. The maintenance of normal *Bmp4* expression in the extra-embryonic region of the embryos serves as an internal control for the in situ procedure.

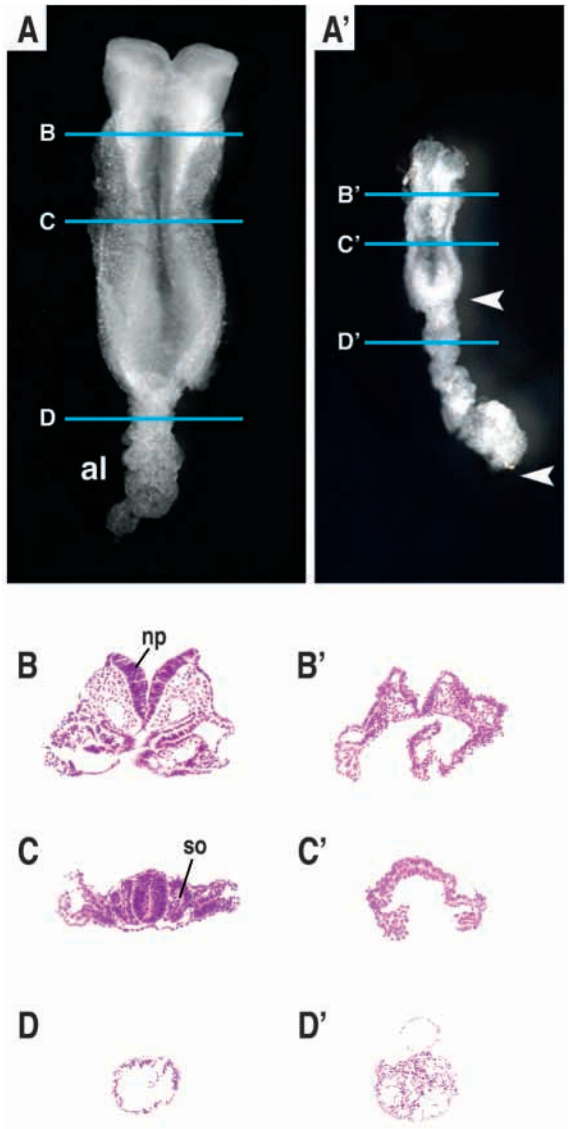

Fig. 2. Gastrulation phenotype of *Chrd*$^{-/-}$ embryos. (A) Wild-type and (A′) mutant embryos at early somite stage. In the mutant, the body is reduced and the allantois (al) proportionally enlarged. (B-D′) Sections through wild-type (B-D) and mutant embryos (B′-D′) at the levels indicated in A and A′. Note the poorly differentiated neural plate (np) of the mutant (B′) and its lack of trunk mesoderm (C′). (D′) The increase in extra-embryonic mesodermal cells in the allantois of the mutant. so, somite.

intermediate and lateral plate mesoderm of the future trunk. The early phenotype of *Chrd*$^{-/-}$ mutants, in which the allantois is expanded at the expense of the embryonic mesoderm, is consistent with an early ventralization of the mouse embryo. This phenotype must lead to death of the affected animals, as no homozygous mutant with abnormal allantois was recovered from dissections at later stages. Analysis of this phenotype with molecular markers was not carried out because so few abnormal embryos were obtained.

Perinatal lethality

Only 49% (95 out of 194) of the expected *Chrd*$^{-/-}$ animals were recovered at birth, all showing the same fully penetrant phenotype. Of these, the majority was stillborn, but a few attempted, unsuccessfully, to inflate their lungs. Externally, homozygous mutant neonates were slightly smaller than their wild-type littermates and showed cyanosis, microcephaly and reduction of the external ear, which was set abnormally close to the eye (Fig. 3A′). Histological examination (Fig. 3B′-C′) revealed the lack of thymus (t, a derivative of the third pharyngeal pouch) and secondary palate (p), and hypoplasia of the internal ear (ie) in the mutants. The anterior lobe and pars intermedia of the pituitary gland (pi), both derived from the dorsal oral ectoderm immediately adjacent to the cephalic border of the anterior endoderm, were normal (Fig. 3C,C′). This defined the rostral limit of the phenotype in the oropharynx, with malformations restricted to derivatives of the *Chrd*-expressing endoderm. The thyroid gland, which forms in ventral pharyngeal endoderm at the foramen caecum, did differentiate but was hypoplastic and of irregular shape (th, Fig. 3C′). The parathyroid glands, derivatives of pharyngeal pouches 3 and 4, were absent (data not shown), an observation consistent with the neonatal hypocalcaemia seen in individuals with DiGeorge syndrome (DiGeorge, 1968). We conclude that the phenotype of *Chrd*$^{-/-}$ stillborn mice recapitulates most of the features described in such individuals.

Skeletal defects

In skeletal preparations of *Chrd*$^{-/-}$ newborn animals, the appendicular and lumbar bones were normal, but the base of the skull and the anterior axial skeleton presented multiple defects. Alterations in the temporal bone included lack of the squama temporalis (st) and shortening of the zygomatic arch (Fig. 4A,A′). We also observed a considerable hypoplasia of the hyoid bone and of the thyroid and cricoid laryngeal cartilages (Fig. 4B′), and an abnormally small jaw (Fig. 4C′). In the base of the skull, the alisphenoid (as) appeared normal, but in the midline the basioccipital (bo) and basisphenoid (bs) bones were fused, and the presphenoid (ps) was hypoplastic (Fig. 4D,D′). Consistent with the histological findings, the palatine shelves failed to extend medially to form the secondary palate. In the ear, the tympanic ring and otic capsule were reduced and malformed (Fig. 4D′). Skeletal malformations were also observed in cervical and thoracic regions of the vertebral column. Vertebral bodies (vb) were smaller in *Chrd*$^{-/-}$ neonates (Fig. 4E′), with delayed ossification and occasional loss of other elements of the vertebrae such as spinous processes, neural arches and the anterior arch of the atlas (Fig. 4E′ and Fig. 5A′).

The skeletal defects of *Chrd* mutants were already detectable in cartilage condensations at E14.5 (Fig. 5A,A′). The basioccipital and basisphenoid cartilages were fused, and the ossification centre of the basioccipital was narrower and extended into the basisphenoid (Fig. 5B,B′). The anterior notochord, which was present in the midline of the wild-type basioccipital, was absent in *Chrd* mutants (Fig. 5B,B′). The absence of anterior notochord was confirmed by histological examination of the cervical region at E14.5 (Fig. 5F′).

The bones affected by the *Chrd* mutation have very different origins. The basioccipital is purely of somitic origin; parts of the basisphenoid arise from endochondral ossification of cephalic mesenchyme; the palatine originates from

intramembranous ossification of neural crest-derived mesenchyme; the otic capsules differentiate from a mix of paraxial mesoderm and neural crest cells; and the hyoid is strictly neural crest derived (Le Douarin and Kalcheim, 1999). Amid such diversity of lineages, the unifying principle of the phenotype seems to be the location of malformed structures in the proximity of the *Chrd*-expressing axial mesendoderm (Fig. 1E). This interpretation is consistent with the observed premature degeneration of the anterior notochord in *Chrd*$^{-/-}$ animals, and with the requirement of prechordal plate and mesendoderm derived signals for the development of the

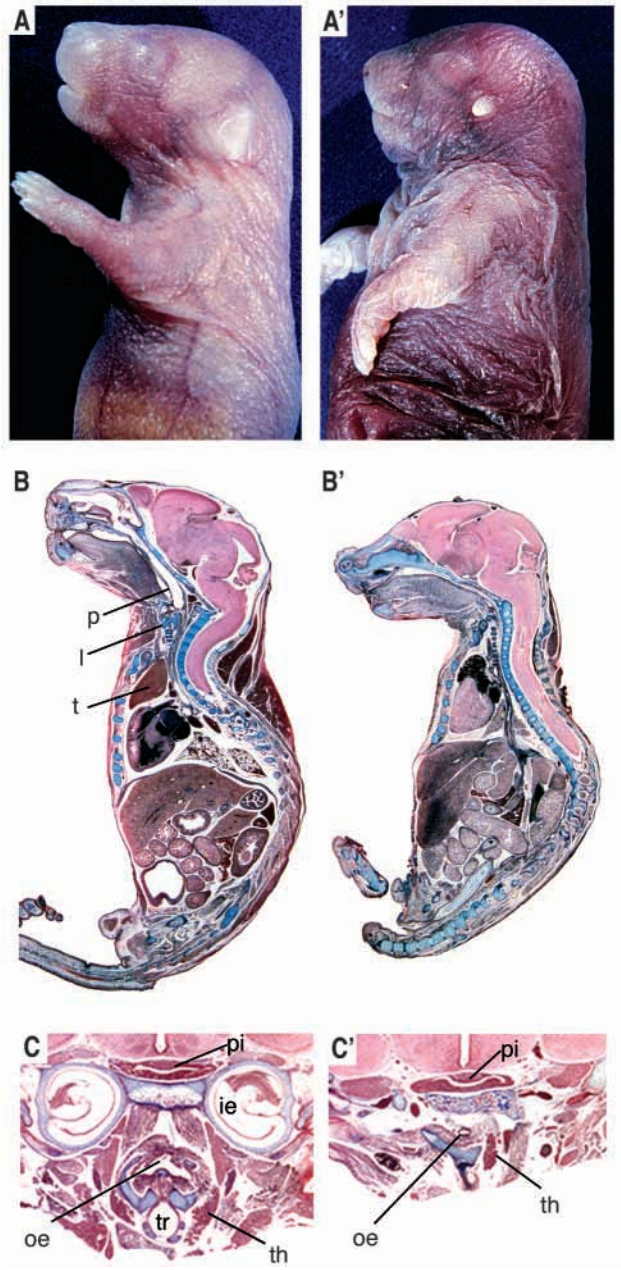

Fig. 3. Morphological and histological analysis of *Chrd*$^{-/-}$ newborn mice. (A,A′) External appearance of wild-type (A) and homozygous mutant (A′) mice. The mutants appear cyanotic; their external ear is reduced and set closer to the eye than in wild type. (B,B′) Sagittal sections of wild-type (B) and mutant (B′) mice. In the mutant, the secondary palate (p) and thymus (t) are absent and the laryngeal cartilages (l) are severely reduced in size. The overall morphology and size of the central nervous system was not affected. (C,C′) Coronal sections of wild-type (C) and mutant (C′) mice at the level of the neck. Note the absence of the inner ear (ie) and oesophagus (oe), and the reduction in size of the trachea (tr) and thyroid (th). pi, pituitary gland.

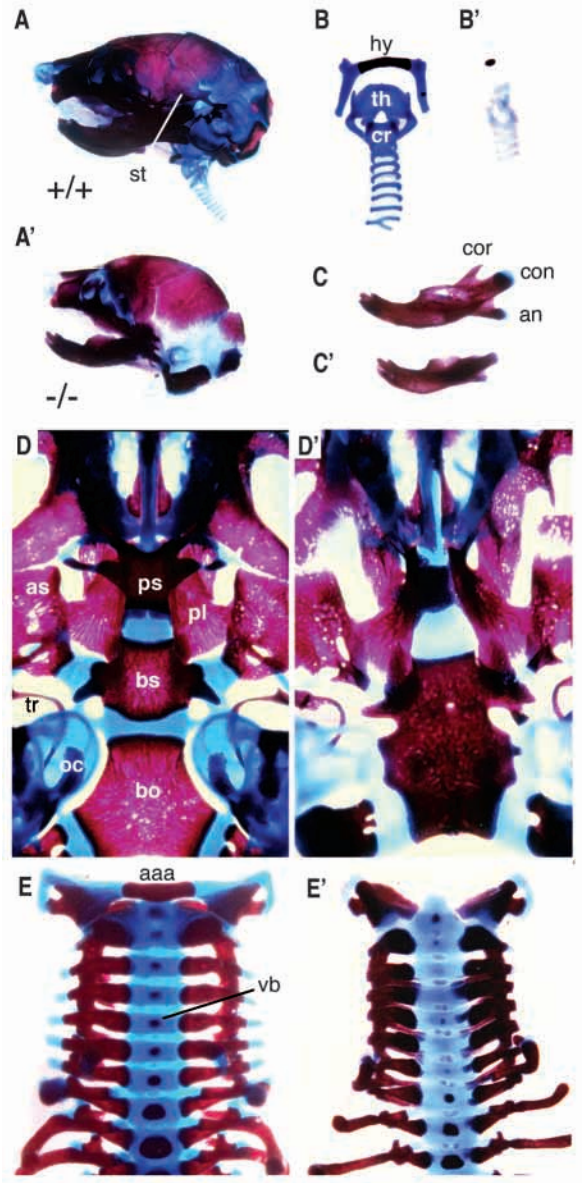

Fig. 4. Skeletal preparations of wild-type and mutant neonates. (A-E) Wild-type neonates. (A′-E′) Mutant littermates. Bone is stained with Alizarin Red and cartilage with Alcian Blue. (A,A′) Lateral view of the skull showing microcephaly and the lack of the squama temporalis (st) in the mutant (A′). (B,B′) Tracheal and laryngeal cartilages in the wild type (B) and mutant (B′); th, thyroid; cr, cricoid cartilages; hy, Hyoid bone. (C,C′) Lateral view of the mandibles; note the lack of the coronoid (cor), condylar (con) and angular (an) processes in the mutant (C′) jaw. (D,D′) Dorsal view of the base of the skull. as, alisphenoid; pl, palatine; ps, presphenoid; bs, basisphenoid; bo, basioccipital; tr, tympanic ring; oc, otic capsule. (E,E′) Ventral view of the cervical vertebral column. The anterior arch of the atlas (aaa) is missing in the mutant and the ossification centres of the vertebral bodies (vb) are reduced.

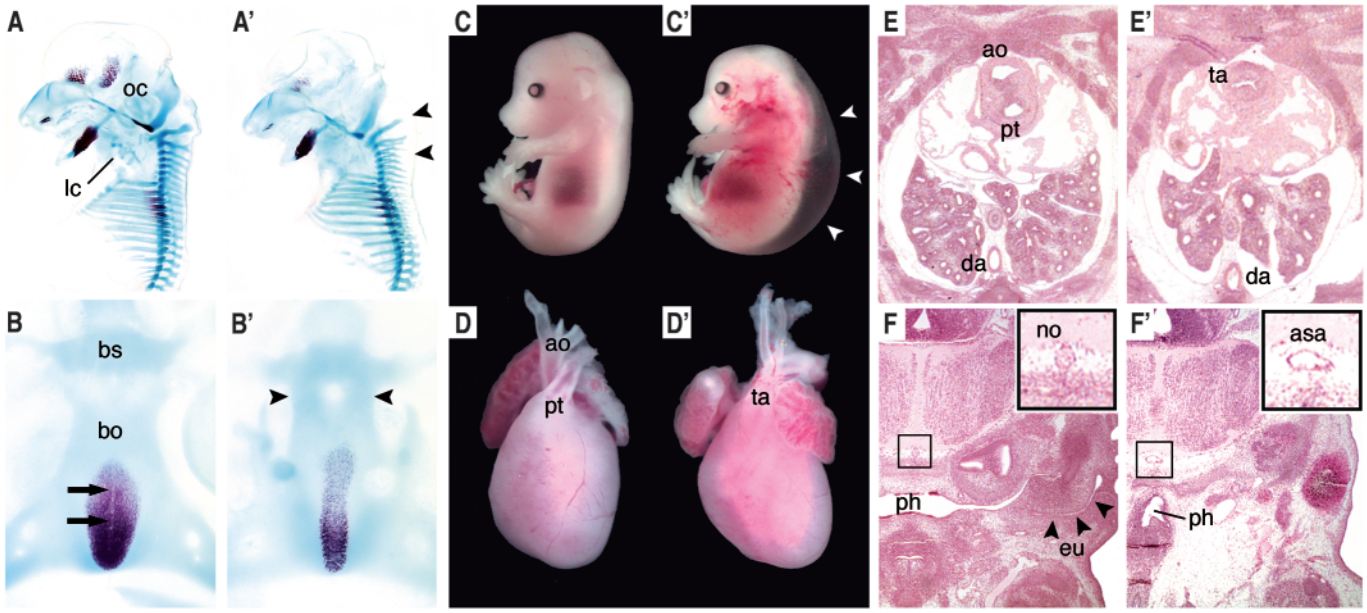

Fig. 5. Phenotype of *Chrd*$^{-/-}$ embryos at E14.5. (A,A′) Skeletal preparation of wild-type (A) and (A′) mutant littermates. Arrowheads in A′ indicate underdeveloped vertebral neural arches. (B,B′) Dorsal view of the base of the cranium. Arrows in B indicate the presence of the anterior notochord. Arrowheads in B′ indicate the cartilaginous bridge that links the primordia of the basisphenoid (bs) and basioccipital bones (bo). oc, otic capsule; lc, laryngeal cartilages. (C,C′) External view of wild-type (C) and mutant (C′) animals. Note the severe oedema (arrowheads) and haemorrhage in the *Chrd*$^{-/-}$ embryo. (D,D′) Wild-type (D) and *Chrd*$^{-/-}$ (D′) mutant hearts. ao, aorta; pt, pulmonary trunk; ta, truncus arteriosus. (E-F′) Coronal sections of wild-type (E,F) and mutant (E′,F′) embryos. In the thorax of the mutant (E′) the undivided truncus arteriosus is clearly visible. In the mutant, an enlarged anterior spinal artery (asa, inset in F′) is seen instead of a notochord (no). Note the striking reduction of the pharynx (ph) and the absence of the eustachian tube (eu) in the mutant. da, descending aorta.

skeleton of the head (Belo et al., 1998; Couly et al., 2002; David et al., 2002).

DiGeorge-like cardiovascular defects

The cyanosis observed at birth can be a sign of cardiac malfunction. To investigate this further, dissections at different stages of embryonic development were performed. At E14.5, the hearts of *Chrd*$^{-/-}$ animals showed a single vessel, instead of the normal two, in the cardiac outflow tract (Fig. 5D,D′,E,E′). This condition is known in humans as persistent truncus arteriosus and is an important malformation in individuals with DiGeorge syndrome. The lack of separation between the ascending aorta and the pulmonary trunk may increase the working load of the right ventricle causing its hypertrophy, as well as the vasodilatation, oedema and haemorrhage seen in E14.5 embryos (Fig. 5C′). As in DiGeorge syndrome, defects in the cardiovascular system extended beyond the outflow tract and included the great vessels derived from the pharyngeal arch arteries (Fig. 6). In newborn *Chrd* mutants, the common carotid arteries directly joined the truncus arteriosus, resulting in the absence of the brachiocephalic artery and part of the aortic arch (Fig. 6A-C). The pulmonary arteries originated directly from the proximal truncus arteriosus, resulting in the absence of a common pulmonary trunk (Fig. 6A-C). In addition, laterality defects were observed, with an abnormal right turning of the aorta in 40% of the mutants (Fig. 6, compare 6E with 6F). When dissections were performed from the posterior, it could be seen that, depending of the laterality of the descending aorta, the right or left subclavian arteries adopted an abnormal retro-oesophageal position (Fig. 6D-F). Similar defects have been described in chick embryos with neural crest cells ablations (Kirby et al., 1983), and in mice carrying deletions in the DiGeorge congenic region (Lindsay et al., 1999; Merscher et al., 2001) or mutations in *Tbx1* and *Fgf8* (Abu-Issa et al., 2002; Frank et al., 2002; Jerome and Papaioannou, 2001; Lindsay et al., 2001; Vitelli et al., 2002b).

At birth, only 49% of the expected *Chrd* homozygous mutants were recovered. However, 48 of the expected 56 (86%) *Chrd*$^{-/-}$ embryos were still alive in litters dissected at E14.5, a frequency not significantly different from that observed at E8.5 (88%). The sharp increase in lethality after E14.5 coincides with the full manifestation of the cardiovascular phenotype, and suggests that circulatory malfunction is an important cause of lethality of *Chrd*$^{-/-}$ embryos during late gestation.

Pharyngeal abnormalities

To determine the onset of the pharyngeal phenotype we dissected pregnant females from heterozygous matings at different times post coitum. At E9.0, a stage at which *Chrd* is expressed in the pharyngeal endoderm, *Chrd*$^{-/-}$ embryos could be identified by an indentation in the neck region (Fig. 7A′, arrow). The otic vesicles of the mutants were reduced to half their normal diameter (Fig. 7A′, arrowheads) and the second (hyoid) pharyngeal arch was missing. Pharyngeal arches three to six never formed in mutant embryos (Fig. 7B′ and data not shown). The missing or malformed structures are either direct precursors or play inductive roles during the development of many of the organs that are defective at birth in *Chrd*$^{-/-}$ mice. As most of the phenotypic abnormalities observed in newborn

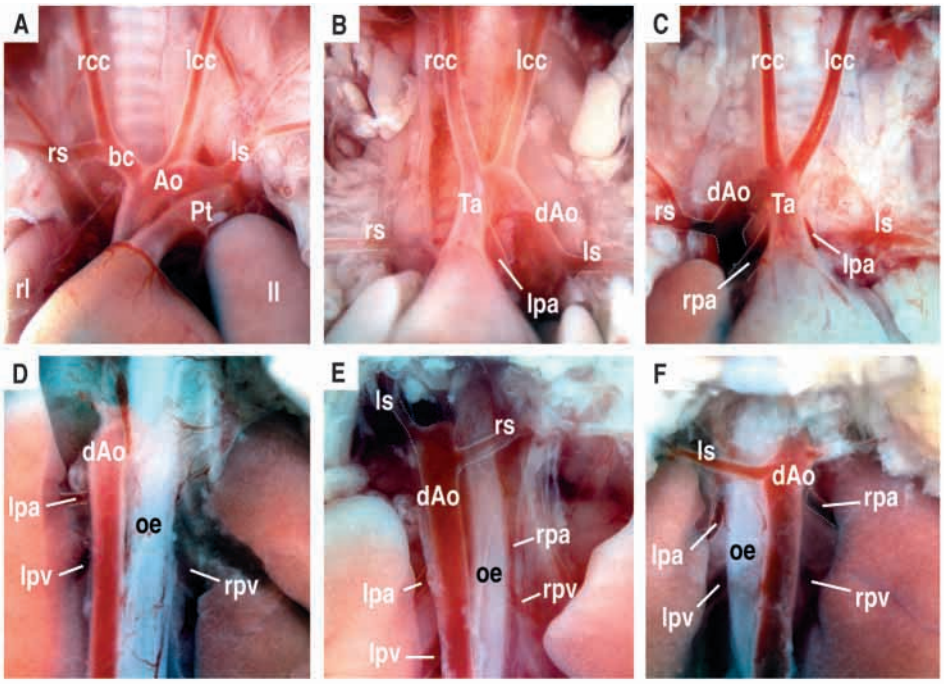

Fig. 6. Arterial defects in *Chrd*$^{-/-}$ newborns. Frontal (A-C) and posterior (D-F) views of the outflow tract and great vessels of wild-type (A,D) and two *Chrd*$^{-/-}$ (B,C,E,F) neonates. The auricles have been removed to facilitate observation. In the wild-type (A,D) the aorta (Ao) and the pulmonary trunk (Pt) are separate. The aorta begins at the left ventricle and turns to the left. The descending aorta (dAo) is located on the left side of the oesophagus (oe). The brachiocephalic artery (bc) branches from the right side of the aortic arch giving rise to the right common carotid (rcc) and the right subclavian arteries (rs). The left common carotid (lcc) and the left subclavian (ls) emerge directly from the aortic arch. (B,E) Mutant animal with left-turning aortic arch. The left and right common carotids originate in the truncus arteriosus (Ta). The brachiocephalic artery is absent and the right subclavian is abnormally located posterior to the oesophagus. The left (lpa) and right (rpa) pulmonary arteries arise from the most proximal part of the truncus. (C,F) Mutant animal with right-turning aortic arch. Forty percent of the mutants present abnormal right turning of the aorta. The descending aorta is placed on the right side of the oesophagus and the left subclavian runs posterior to it. Several vessels have been outlined to facilitate observation. rl, right lung; ll, left lung; lpv, left pulmonary vein; rpv, right pulmonary vein.

mutants have their embryological origin in the pharyngeal endoderm and the peripharyngeal region, we analyzed the expression of a number of genes known to have important developmental roles in human hereditary disease.

We examined first the expression of *Pax3*, a transcription factor expressed in neural crest, dorsal neural tube and somites (Goulding et al., 1991). In humans, *PAX3* is mutated in neural crest diseases designated Waardenburg syndrome types 1 and 3 (Strachan and Read, 1994) and is a co-regulator, together with *SOX10*, of the microphthalmia or *MITF* gene (Bondurand et al., 2000), the transcription factor mutated in Waardenburg syndrome type 2a in humans (Tassabehji et al., 1994). Mutation of *Pax3* in the splotch (*Sp*^{2H}) mouse results in heart defects, including persistent truncus arteriosus, as well as malformation of the thymus, thyroid and parathyroid glands (Conway et al., 1997). We found that *Pax3* expression was indistinguishable between mutant and wild-type embryos at E7.5 (not shown), but at E10.5 significant differences were observed. The *Pax3*-positive neural crest cells that migrate through pharyngeal arches 3, 4 and 6 (Fig. 7C, arrowheads) were barely detectable in *Chrd*$^{-/-}$ animals (Fig. 7C′). These neural crest cells populate the septum separating the aorta from the pulmonary artery in the outflow tract, or conotruncal region, of the heart (Li et al., 2000). The failure of cardiac neural crest to reach the heart explains the lack of outflow tract septation and the subsequent cardiovascular phenotype observed in *Chrd* mutants. Interestingly, expression of Pax3 in other tissues such as the mandibular (md) component of the first pharyngeal arch, dermomyotomes (dm) and myoblast precursors in the forelimbs (fl) was unaffected (Fig. 7C′).

Next, we performed in situ hybridizations with *Sox10*, a gene mutated in individuals with Waardenburg syndrome type 4 (Pingault et al., 1998) that is expressed in neural crest and Schwann cells. At E7.5, the expression of *Sox10* was the same in *Chrd*$^{-/-}$ embryos and in their wild-type littermates (data not shown). At E9.5, *Sox10* expression in the dorsal root ganglia (drg) of the trunk was normal (Fig. 7B,B′), but the distribution of glial cells expressing *Sox10* revealed specific defects in the organization of the peripheral nervous system in the neck and head region of the mutants (Fig. 7B′). In particular, cranial sensory ganglia showed marked abnormalities. The trigeminal (tr) and vestibulo-cochlear (vc) ganglia, corresponding to the V and VIII cranial nerves, respectively, were located closer together in *Chrd*$^{-/-}$ embryos than in wild-type littermates. In addition, abnormal nerve projections connecting the two of them were seen (Fig. 7B′, arrowhead). The geniculate (g), petrosal (p) and nodose (n) ganglia, corresponding to cranial nerves VII, IX and X, were the most affected, showing either an extreme reduction in size or complete absence. These three ganglia originate from the epibranchial placodes, and are known to require inductive signals from anterior endoderm for their proper development (Begbie et al., 1999). The lack of epibranchial placode-derived ganglia indicates that the secreted protein Chrd is required for the activity of the inductive signal released by pharyngeal endoderm.

Pax9 is a transcription factor required for the development of the pharyngeal endoderm and its derivatives in the mouse (Peters and Balling, 1999; Peters et al., 1998). At E9.5, expression of *Pax9* in the pharyngeal endoderm of *Chrd*$^{-/-}$ embryos was weaker than in their wild-type littermates (pe, Fig. 7D,D′). *Pax9* expression revealed that the size and shape of the pharynx was altered in the *Chrd* mutants, with pharyngeal pouches reduced to a single swelling in the anterior-most region (Fig. 7E,E′). The hypoplasia of the pharynx was confirmed by histological sections of E14.5

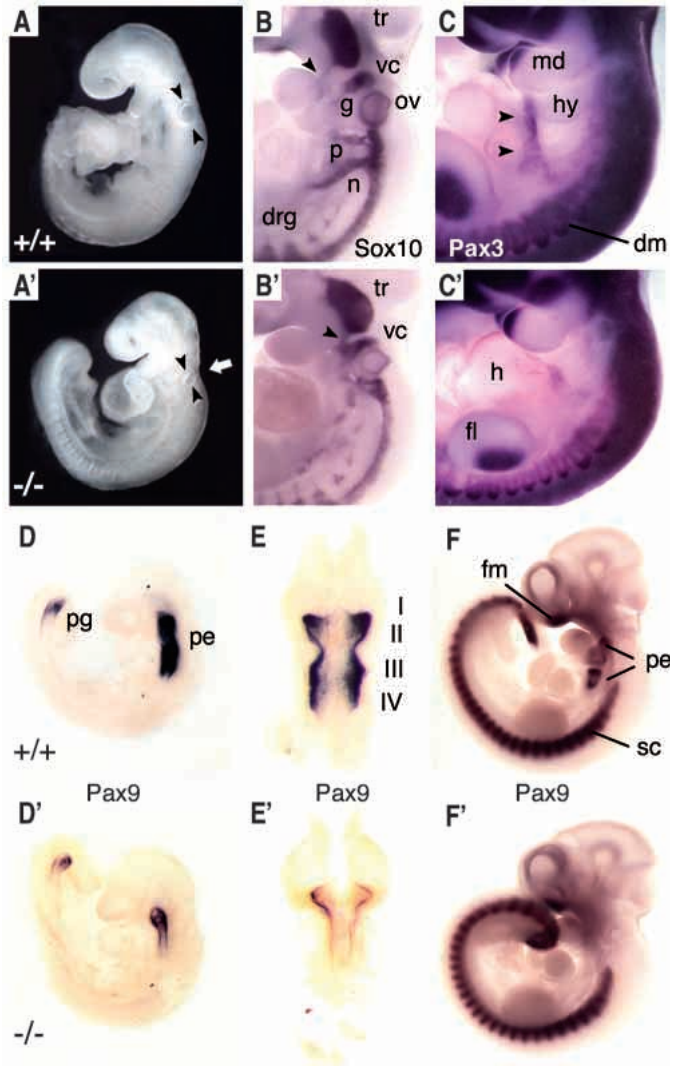

Fig. 7. Pharyngeal defects in *Chrd*$^{-/-}$ embryos at mid-gestation. (A,A′) External view of wild-type (A) and mutant (A′) E9.0 embryos; mutants present a fully penetrant phenotype consisting in reduction of the otic vesicle (arrowheads), absence of second (hyoid) pharyngeal arch and a conspicuous indentation in the neck (arrow). (B,B′) Whole-mount in situ hybridization of E9.5 embryos with a *Sox10* probe that labels glial cells. The trigeminal (tr) and vestibulo-cochlear (vc) ganglia are deformed and displaced in the mutant (B′). (C,C′) *Pax3* whole-mount in situ hybridization of E10.5 embryos. Neural crest cells (arrowheads) migrating through the peripharyngeal region into the proximity of the heart (h) are absent in the mutant embryo (C′). md, mandibular component of the first pharyngeal arch; hy, hyoid or second pharyngeal arch; dm, dermomyotomes; fl, forelimb. Abnormal axonal projections from the trigeminal into the vestibulo-cochlear are indicated (arrowhead). The epibranchial placode-derived geniculate (g), petrosal (p) and nodose (n) ganglia are absent in the mutant. ov, otic vesicle; drg, dorsal root ganglia. (D-F′) Whole-mount in situ hybridization with *Pax9* probe. (D,D′) Lateral view of E9.5 wild-type (D) and mutant (D′) embryos made transparent with benzyl benzoate. *Pax9* pharyngeal expression is reduced in the mutant. pe, pharyngeal endoderm; pg, postanal gut. (E,E′) Dorsal view of the same embryos; in the mutant the pharynx is reduced and pharyngeal pouches II, III and IV are absent. (F,F′) Lateral view of E10.5 wild-type and mutant embryos. Note the lack of *Pax9* expression specifically in pharyngeal endoderm (pe) of the mutant. fm, facial mesenchyme; sc, sclerotome.

embryos, in which the anterior endoderm appeared as a thin tube outlining a greatly diminished lumen (ph, Fig. 5F,F′). The reduction of pharyngeal endoderm has also been observed in *Xenopus Chrd* knockdowns (Oelgeschläger et al., 2003). Non-pharyngeal regions in which *Pax9* mRNA is normally expressed, such as the somitic sclerotomes (sc) and facial mesenchyme (fm), did not show differences in the distribution or abundance of the transcripts (Fig. 7F,F′).

We conclude from these studies that alterations in *Pax3*, *Sox10* and *Pax9* expression are restricted to a very limited area of wider expression domains, suggesting that lack of the secreted protein Chrd specifically disrupts local regulatory pathways acting in the peripharyngeal region surrounding the *Chrd*-expressing endoderm.

Tbx1 and *Fgf8* expression requires chordin

To study the interaction of *Chrd* with genes known to cause DiGeorge or DiGeorge-like phenotypes in mice, we analyzed the expression of *Tbx1* and *Fgf8* in *Chrd* mutant embryos. *Tbx1* is a member of the T-box family of transcription factors (Papaioannou and Silver, 1998). It maps within the DGS/VCFS 22q11 microdeletion in humans and has recently been shown to cause DiGeorge-like phenotype upon inactivation in mice (Jerome and Papaioannou, 2001; Lindsay et al., 2001; Merscher et al., 2001; Vitelli et al., 2002a). Expression of *Tbx1* was altered in *Chrd*$^{-/-}$ embryos. In wild-type E7.5 animals, *Tbx1* is expressed in the foregut (future pharyngeal endoderm) and head mesoderm (Fig. 8A). At this stage, mutant littermates showed a clear reduction in the levels of *Tbx1* expression in the same areas (Fig. 8A′). The reduction in *Tbx1* mRNA was equally clear in the pharyngeal region of *Chrd* homozygous embryos at E8.0, E8.5 and E9.0 (Fig. 8B′,C′,D′). Transverse histological sections showed that at the cellular level the abundance of *Tbx1* transcripts was drastically reduced in endoderm, both in the pharynx and foregut up to the level of the hepatic diverticulum (Fig. 8F-H′) Diminution in the concentration of *Tbx1* mRNA was also evident in mesoderm, including head, splanchnic (arrowheads) and somatic mesoderm (arrows) in the peripharyngeal region (Fig. 8F′,G′,H′). In addition, *Tbx1* expression at E9 in the mesodermal core of the first pharyngeal arch was diffuse, extending to most of the arch, and *Tbx1* transcripts were absent from the otic vesicle (Fig. 8D-D′).

Fgf8 is a secreted growth factor expressed in a variety of tissues, including the pharyngeal endoderm and neighboring mesoderm (Crossley and Martin, 1995; MacArthur et al., 1995). During early development, *Fgf8* is required for gastrulation (Sun et al., 1999) and the establishment of the left/right axis of symmetry (Meyers and Martin, 1999). At later stages of *Fgf8* is required for limb (Lewandoski et al., 2000; Moon and Capecchi, 2000) and craniofacial (Trumpp et al., 1999) development. Recent experiments have shown that mice with reduced *Fgf8* activity present a spectrum of cardiovascular and pharyngeal defects that closely mimic DiGeorge syndrome (Abu-Issa et al., 2002; Frank et al., 2002). In addition, *Fgf8* expression is abolished in the pharyngeal endoderm of *Tbx1*$^{-/-}$ mutants and both genes interact genetically during the differentiation of the pharyngeal arch arteries (Vitelli et al., 2002b). At E9, *Fgf8* expression in *Chrd* mutants is normal in the mid-hindbrain isthmus, frontonasal prominence and tail. However, in pharyngeal endoderm, *Fgf8* transcript levels are

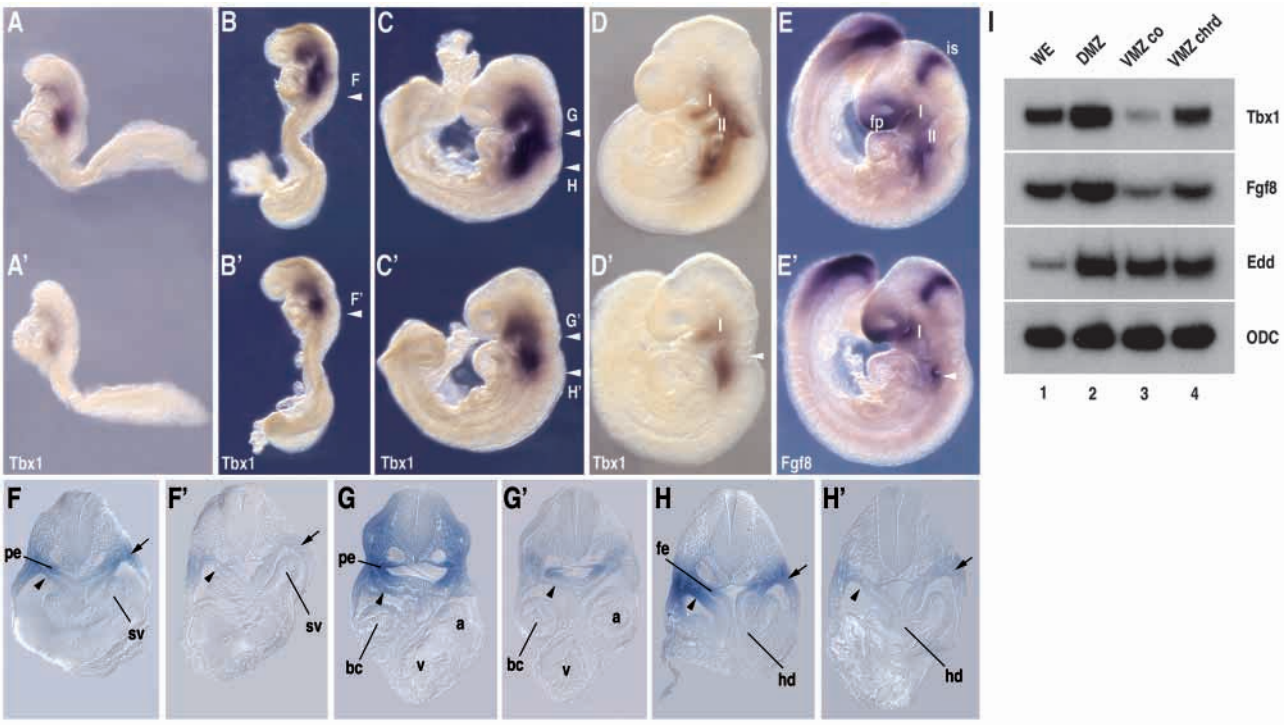

Fig. 8. *Chrd* regulates *Tbx1* and *Fgf8* expression in mutant mice and *Xenopus* ventral marginal zones. (A-E) Wild-type embryos. (A′-E′) Mutant littermates. In mutants, the levels of *Tbx1* expression are diminished at E7.5 (A,A′), E8.0 (B,B′), E8.5 (C,C′) and E9 (D,D′). Arrowheads indicate the level of sections depicted in F-H′. At E9 *Tbx1* transcripts are absent of otic vesicle (arrowhead in D′). At E9, *Fgf8* expression in the mutant endoderm has disappeared and mesodermal expression is restricted to a small area in the most posterior part of the neck (arrowhead in E′). (F-H′) Nomarski optic photographs of section through wild-type (F-H) and *Chrd* mutant littermates (F′-H′). Note the reduction of *Tbx1* expression in the splanchnic (arrowheads) and somatic mesoderm (arrows), as well as in the mesenchyme of the head and peripharyngeal region. I, first pharyngeal arch; II, second pharyngeal arch; fp, frontonasal prominence; is, isthmus; pe, pharyngeal endoderm; sv, sinus venosus; bc, bulbus cordis; v, ventricular chamber; a, atrial chamber; fe, foregut endoderm; hd, hepatic diverticulum. (I) *Xenopus* VMZ assays. RT-PCR analyses of RNAs isolated from whole embryos (WE), dorsal marginal zones (DMZ), uninjected ventral marginal zones (VMZ co) and *Chrd* injected ventral marginal zones (VMZ chrd). *Tbx1* and *Fgf8* transcripts are high in the whole embryo and DMZ, but not in uninjected VMZ (lanes 1, 2 and 3, respectively). Lane 4 shows that *Tbx1* and *Fgf8* are induced in VMZs by *Chrd* injection. Note that the levels of endodermin (Edd), a pan-endodermal marker, are not affected. Ornithine decarboxylase (ODC) is expressed uniformly during embryonic development and serves as a loading control.

drastically reduced (Fig. 8E′). The reduction of *Tbx1* and *Fgf8* expression in *Chrd*$^{-/-}$ embryos suggested that both genes act downstream of *Chrd* in the same regulatory pathway. These experiments do not determine whether *Chrd* is required for the maintenance or for the induction of *Tbx1* and *Fgf8* in the pharynx and neighboring tissues.

To test whether *Chrd* can induce *Tbx1* and *Fgf8*, we injected *Chrd* mRNA (50 pg) into the ventral region of *Xenopus* embryos at the four-cell stage. Ventral marginal zone (VMZ) explants were dissected at early gastrula, cultured until sibling embryos reached early neurula stage, and analyzed by RT-PCR. *Tbx1* and *Fgf8* mRNAs were expressed at high levels in whole embryos and dorsal marginal zone (DMZ) explants at this stage, and at low levels in VMZ explants (Fig. 8I, lanes 1-3). Upon microinjection, *Chrd* mRNA increased the levels of *Tbx1* and *Fgf8* in VMZ (Fig. 8I, lane 4). In situ hybridization of microinjected *Xenopus* embryos confirmed that the *Tbx1* transcripts induced by *Chrd* mRNA were located in pharyngeal endoderm (data not shown). We conclude that *Chrd*, a Bmp antagonist, can induce *Tbx1* and *Fgf8* expression in *Xenopus* embryos, and is required for full expression of these genes in the pharyngeal region of the mouse embryo.

DISCUSSION

Inactivation of the *Chrd* gene has multiple effects on mouse development. At early stages mutation of *Chrd* can ventralize the murine gastrula with low penetrance. In embryos that survive this potentially lethal phase, lack of Chrd impairs the development of the pharynx and organs derived from it. Secretion of Chrd protein by anterior mesendoderm is required for the development of the pharynx itself, as well as for the patterning of the mesoderm and neural crest of the peripharyngeal region and the induction of the epibranchial placodes. Loss of Chrd function has phenotypic effects very similar to those of DiGeorge syndrome, despite the *Chrd* gene being located outside the 22q11 deletion interval. The defects seen in endoderm, mesoderm, neurectodermal placodes and neural crest of the head and neck region correlate with abnormal expression patterns of important developmental regulators such as *Sox10*, *Pax3*, *Pax9*, *Tbx1* and *Fgf8*.

Chrd and early development

As Chrd functions by regulating the access of Bmps to their receptors, the effects of *Chrd* inactivation must result, at least

initially, from altered Bmp signaling. During late gastrulation Bmp2, Bmp4, Bmp5, Bmp6 and Bmp7 are co-expressed in posterior mesoderm. Embryos that are homozygous mutant for either Bmp2 or Bmp4, or double homozygous mutant for Bmp5 and Bmp7, show severe reduction or absence of the allantois (Fujiwara et al., 2001; Solloway and Robertson, 1999; Zhang and Bradley, 1996). This phenotype is the opposite of the one described here, in which expansion of the allantois at the expense of the embryonic mesoderm was observed in *Chrd*$^{-/-}$ embryos at early somite stages (Fig. 2). This suggests that the lack of Chrd leads to an increase in Bmp signaling and a subsequent shift in the differentiation of the trunk mesoderm towards a more ventroposterior fate.

Chrd is not the only Bmp antagonist expressed at these stages. Other proteins with possible Bmp antagonist activity, such as noggin (McMahon et al., 1998), follistatin (Iemura et al., 1998) and bambi (Grotewold et al., 2001) could collaborate in opposing the ventralizing activity of Bmps. The existence of these potentially redundant genes may explain the low penetrance or absence of ventralization observed when Bmp antagonists are individually inactivated. In the case of *Chrd*;*Nog* double homozygous mutants, ventralized embryos with large allantois were also observed at the neural fold stage, although with more severe phenotypes (Bachiller et al., 2000). The existence of a gastrulation phenotype in *Chrd*$^{-/-}$ embryos indicates that the early functional compensation provided by *Nog* or other Bmp inhibitors is not completely penetrant in *Chrd* mutants.

Chrd is required for pharyngeal development

The first manifestations of the post-gastrulation Chrd phenotype occur at E8.5-9, at the pharyngula stage. At this time in development *Chrd* is expressed in dorsal foregut and notochord (Fig. 1E), and various Bmps are expressed in the surrounding head and neck region (Dudley and Robertson, 1997). Bmps are potent growth factors involved in embryonic induction, cellular differentiation and apoptosis. Their signals regulate the expression of variety of transcription factors, among them several members of the Pax and Tbx families (Peters and Balling, 1999; Rodriguez-Esteban et al., 1999; Yamada et al., 2000). As a consequence of Chrd deficiency, the expression of *Tbx1* is reduced in the pharyngeal endoderm of *Chrd*$^{-/-}$ mutants (Fig. 8).

We propose that *Tbx1* mediates the autocrine effect of Chrd on the endoderm, subsequently affecting the formation of the thymus, parathyroid glands and other pharyngeal endoderm derivatives that are defective in *Tbx1*$^{-/-}$ (Jerome and Papaioannou, 2001; Lindsay et al., 2001; Merscher et al., 2001) and *Chrd*$^{-/-}$ mice (this work). As development progresses, the endodermal component of the DiGeorge phenotype may be aggravated by the reduction of *Pax9* and *Fgf8* expression in pharyngeal endoderm (Fig. 7E′,F′), for *Pax9* mouse mutants lack derivatives of the pharyngeal pouches (Peters et al., 1998), and mice with reduced *Fgf8* activity present DiGeorge-like phenotypes (Abu-Issa et al., 2002; Frank et al., 2002). It has been shown that *Fgf8* expression is eliminated from the endoderm of *Tbx1*$^{-/-}$ mutants (Vitelli et al., 2002b), and therefore the decrease in *Tbx1* levels observed in *Chrd*$^{-/-}$ embryos could explain the phenotype observed. However, our experiments do not exclude the possibility that *Chrd* may also control *Fgf8* and other endoderm expressed genes through a parallel *Tbx1*-independent route. Additional experiments will also be required to explore the existence of a possible regulatory loop linking the maintenance of *Chrd* expression to *Tbx1* activity. The disruption of endoderm development would in turn impair signaling to nearby ectoderm (Begbie et al., 1999), preventing the induction of the epibranchial placodes, which are missing in *Chrd*$^{-/-}$ embryos (Fig. 7B′).

Chrd and skeletal development

The striking similarities between the *Chrd*$^{-/-}$ and *Tbx1*$^{-/-}$ phenotypes, and the reduction of *Tbx1* expression in the head mesoderm of *Chrd* mutants, suggest that *Tbx1* may also be a mediator of the paracrine effects of Chrd on peripharyngeal mesoderm. Although at first inspection most of the defects observed in this area seem to involve derivatives of the neural crest, the phenotypes in the base of the skull and rostral vertebral column suggest that some of the structures affected are of head mesoderm or somitic origin, and thus derived from *Tbx1*-expressing paraxial mesoderm. A further indication that some of the defects observed in the peripharyngeal region of the *Chrd*$^{-/-}$ animals originate in the mesoderm independently of the neural crest, is provided by a comparison with the phenotype of the endothelin A receptor (*Ednra*) mutation in mouse (Clouthier et al., 1998). Ednra activity is cell autonomous in the neural crest, and upon disruption causes cardiac and head and neck defects reminiscent of DGS/VCFS, but does not produce malformations of the axial skeleton as reported here for *Chrd* mutant animals.

Pharyngeal endoderm patterns the neural crest

One of the salient characteristics of DiGeorge syndrome is the presence of persistent truncus arteriosus in the outflow tract of the heart. This phenotype is also seen in mice homozygous for *Sp*^{2H}, a mutation in the *Pax3* gene that affects neural crest migration (Conway et al., 1997). In *Chrd* homozygous mutant embryos, *Pax3* expression is normal in the cranial neural crest, while the cells are still located within the neural folds, but at later stages the migration of *Pax-3*-positive neural crest cells is impaired in the mutants. As *Chrd* is not expressed in neural crest, the abnormalities observed must be secondary to the lack of *Chrd* expression in pharyngeal endoderm. In zebrafish, *one-eye pinhead* (*oep*), *Casanova* (*cas*) and *Van Gogh* (*vgo*) mutants cause defects in the endoderm that interfere with the correct migration of neural crest cells (David et al., 2002; Piotrowski and Nusslein-Volhard, 2000). In the chick, transplantation of pharyngeal endoderm has shown that this tissue instructs Hox-negative neural crest cells to differentiate into particular elements of the head skeleton (Couly et al., 2002). The overall structure of the region through which the neural crest must migrate is disorganized in *Chrd*$^{-/-}$ mutants. In this respect it should be noted that pharyngeal arches 2 to 6 fail to form in these *Chrd* mutants, indicating that Chrd may be particularly important for the patterning of Hox-positive neural crest.

Pharyngeal malformations and Bmp signaling

Chrd maps outside the DiGeorge microdeletion (to human chromosome 3q27) (Pappano et al., 1998) (D.B. and E.M.D.R., unpublished). As DGS/VCFS is not linked in all individuals to deletions in the 22q11 region, the finding that mutations in *Chrd* can reproduce DiGeorge syndrome in mice offers a new

candidate gene for genetic testing in humans. Chrd activity is modulated post-translationally by metalloproteinases (Piccolo et al., 1997) and by other Bmp-binding proteins such as twisted gastrulation (Oelgeschlager et al., 2000) and noggin (Bachiller et al., 2000). Allelic variation in any of these genes, or in components of the Bmp signal transduction pathway could also potentially lead to DiGeorge phenotypes. Furthermore, the realization that multiple components of the Chrd/Bmp pathway may participate in DGS/VCFS might help to explain the considerable phenotypic variability observed in humans and mice with rearrangements in 22q11 (Ryan et al., 1997; Taddei et al., 2001).

The Chrd/Bmp/Noggin signaling system is essential for the establishment of the three major body axes during gastrulation (Bachiller et al., 2000). As shown here, Chrd is also required for patterning the head and neck region of the vertebrate embryo at the pharyngula stage, a time of maximal complexity in the regulatory interactions taking place in the embryo (Raff, 1996). Many congenital malformations have their origin at this particular time in development, which corresponds to the phylotypic stage of the vertebrates (Slack et al., 1993). Further analysis of pharyngeal development will provide a conceptual framework for understanding the role of Chrd/Bmp signaling in the pathogenesis of DiGeorge syndrome and other developmental defects arising in the head and neck region during vertebrate development.

We thank K. Lyons, P. Tam, P. Gruss and J. L. de la Pompa for gifts of plasmids, and R. Gatti, E. Delot and members of our laboratories for comments on the manuscript. This work was supported by the HHMI, NIH, Victor Goodhill Endowment and the Norman Sprague Chair. E.M.D.R. is an investigator of the Howard Hughes Medical Institute.

REFERENCES

Abu-Issa, R., Smyth, G., Smoak, I., Yamamura, K. and Meyers, E. N. (2002). Fgf8 is required for pharyngeal arch and cardiovascular development in the mouse. *Development* **129**, 4613-4625.

Ammann, A. J., Wara, D. W., Cowan, M. J., Barrett, D. J. and Stiehm, E. R. (1982). The DiGeorge syndrome and the fetal alcohol syndrome. *Am J Dis Child* **136**, 906-908.

Bachiller, D., Klingensmith, J., Kemp, C., Belo, J. A., Anderson, R. M., May, S. R., McMahon, J. A., McMahon, A. P., Harland, R. M., Rossant, J. et al. (2000). The organizer factors Chordin and Noggin are required for mouse forebrain development. *Nature* **403**, 658-661.

Begbie, J., Brunet, J. F., Rubenstein, J. L. and Graham, A. (1999). Induction of the epibranchial placodes. *Development* **126**, 895-902.

Belo, J. A., Leyns, L., Yamada, G. and de Robertis, E. M. (1998). The prechordal midline of the chondrocranium is defective in Goosecoid-1 mouse mutants. *Mech. Dev.* **72**, 15-25.

Bondurand, N., Pingault, V., Goerich, D. E., Lemort, N., Sock, E., Caignec, C. L., Wegner, M. and Goossens, M. (2000). Interaction among SOX10, PAX3 and MITF, three genes altered in Waardenburg syndrome. *Hum. Mol. Genet.* **9**, 1907-1917.

Clouthier, D. E., Hosoda, K., Richardson, J. A., Williams, S. C., Yanagisawa, H., Kuwaki, T., Kumada, M., Hammer, R. E. and Yanagisawa, M. (1998). Cranial and cardiac neural crest defects in endothelin-A receptor-deficient mice. *Development* **125**, 813-824.

Conway, S. J., Henderson, D. J. and Copp, A. J. (1997). Pax3 is required for cardiac neural crest migration in the mouse: evidence from the splotch (Sp2H) mutant. *Development* **124**, 505-514.

Couly, G., Creuzet, S., Bennaceur, S., Vincent, C. and le Douarin, N. M. (2002). Interactions between Hox-negative cephalic neural crest cells and the foregut endoderm in patterning the facial skeleton in the vertebrate head. *Development* **129**, 1061-1073.

Crossley, P. H. and Martin, G. R. (1995). The mouse Fgf8 gene encodes a family of polypeptides and is expressed in regions that direct outgrowth and patterning in the developing embryo. *Development* **121**, 439-451.

David, N. B., Saint-Etienne, L., Tsang, M., Schilling, T. F. and Rosa, F. M. (2002). Requirement for endoderm and FGF3 in ventral head skeleton formation. *Development* **129**, 4457-4468.

De Robertis, E. M. and Sasai, Y. (1996). A common plan for dorsoventral patterning in Bilateria. *Nature* **380**, 37-40.

De Robertis, E. M., Larrain, J., Oelgeschlager, M. and Wessely, O. (2000). The establishment of Spemann's organizer and patterning of the vertebrate embryo. *Nat. Rev. Genet.* **1**, 171-181.

DiGeorge, A. M. (1968). Congenital absence of the thymus and its immunologic consequences: concurrence with congenital hypoparathyroidism. In *Immunologic Deficiency Diseases in Man. Birth Defects Original Article Series*, Vol. 4 (ed. D. S. Bergsma and R. A. Good), pp. 116-123. New York, NY: National Foundation Press.

Dudley, A. T. and Robertson, E. J. (1997). Overlapping expression domains of bone morphogenetic protein family members potentially account for limited tissue defects in BMP7 deficient embryos. *Dev. Dyn.* **208**, 349-362.

Francois, V., Solloway, M., O'Neill, J. W., Emery, J. and Bier, E. (1994). Dorsal-ventral patterning of the Drosophila embryo depends on a putative negative growth factor encoded by the short gastrulation gene. *Genes Dev.* **8**, 2602-2016.

Frank, D. U., Fotheringham, L. K., Brewer, J. A., Muglia, L. J., Tristani-Firouzi, M., Capecchi, M. R. and Moon, A. M. (2002). An Fgf8 mouse mutant phenocopies human 22q11 deletion syndrome. *Development* **129**, 4591-4603.

Fujiwara, T., Dunn, N. R. and Hogan, B. L. (2001). Bone morphogenetic protein 4 in the extraembryonic mesoderm is required for allantois development and the localization and survival of primordial germ cells in the mouse. *Proc. Natl. Acad. Sci. USA* **98**, 13739-13744.

Gatti, R. A., Gershanik, J. J., Levkoff, A. H., Wertelecki, W. and Good, R. A. (1972). DiGeorge syndrome associated with combined immunodeficiency. Dissociation of phytohemagglutinin and mixed leukocyte culture responses. *J. Pediatr.* **81**, 920-926.

Goulding, M. D., Chalepakis, G., Deutsch, U., Erselius, J. R. and Gruss, P. (1991). Pax-3, a novel murine DNA binding protein expressed during early neurogenesis. *EMBO J.* **10**, 1135-1147.

Grotewold, L., Plum, M., Dildrop, R., Peters, T. and Ruther, U. (2001). Bambi is coexpressed with Bmp-4 during mouse embryogenesis. *Mech Dev* **100**, 327-330.

Harington, H. (1828-1829). Absence of the thymus gland (Letter to the Editor). *London M. Gaz.* **3**.

Iemura, S., Yamamoto, T. S., Takagi, C., Uchiyama, H., Natsume, T., Shimasaki, S., Sugino, H. and Ueno, N. (1998). Direct binding of follistatin to a complex of bone-morphogenetic protein and its receptor inhibits ventral and epidermal cell fates in early Xenopus embryo. *Proc. Natl. Acad. Sci. USA* **95**, 9337-9342.

Jerome, L. A. and Papaioannou, V. E. (2001). DiGeorge syndrome phenotype in mice mutant for the T-box gene, Tbx1. *Nat. Genet.* **27**, 286-291.

Kirby, M. L. and Bockman, D. E. (1984). Neural crest and normal development: a new perspective. *Anat. Rec.* **209**, 1-6.

Kirby, M. L., Gale, T. F. and Stewart, D. E. (1983). Neural crest cells contribute to normal aorticopulmonary septation. *Science* **220**, 1059-1061.

Lammer, E. J., Chen, D. T., Hoar, R. M., Agnish, N. D., Benke, P. J., Braun, J. T., Curry, C. J., Fernhoff, P. M., Grix, A. W., Jr, Lott, I. T. et al. (1985). Retinoic acid embryopathy. *New Engl. J. Med.* **313**, 837-841.

Larrain, J., Bachiller, D., Lu, B., Agius, E., Piccolo, S. and de Robertis, E. M. (2000). BMP-binding modules in Chordin: a model for signalling regulation in the extracellular space. *Development* **127**, 821-830.

Le Douarin and Kalchiem, C. (1999). *The Neural Crest.* Cambridge: Cambridge University Press.

Lewandoski, M., Sun, X. and Martin, G. R. (2000). Fgf8 signalling from the AER is essential for normal limb development. *Nat. Genet.* **26**, 460-463.

Li, J., Chen, F. and Epstein, J. A. (2000). Neural crest expression of Cre recombinase directed by the proximal Pax3 promoter in transgenic mice. *Genesis* **26**, 162-164.

Lindsay, E. A., Botta, A., Jurecic, V., Carattini-Rivera, S., Cheah, Y. C., Rosenblatt, H. M., Bradley, A. and Baldini, A. (1999). Congenital heart disease in mice deficient for the DiGeorge syndrome region. *Nature* **401**, 379-383.

Lindsay, E. A., Vitelli, F., Su, H., Morishima, M., Huynh, T., Pramparo, T., Jurecic, V., Ogunrinu, G., Sutherland, H. F., Scambler, P. J. et al. (2001). Tbx1 haploinsufficieny in the DiGeorge syndrome region causes aortic arch defects in mice. *Nature* **410**, 97-101.

MacArthur, C. A., Lawshe, A., Xu, J., Santos-Ocampo, S., Heikinheimo, M., Chellaiah, A. T. and Ornitz, D. M. (1995). FGF-8 isoforms activate receptor splice forms that are expressed in mesenchymal regions of mouse development. *Development* **121**, 3603-3613.

McMahon, J. A., Takada, S., Zimmerman, L. B., Fan, C. M., Harland, R. M. and McMahon, A. P. (1998). Noggin-mediated antagonism of BMP signaling is required for growth and patterning of the neural tube and somite. *Genes Dev.* **12**, 1438-1452.

Merscher, S., Funke, B., Epstein, J. A., Heyer, J., Puech, A., Lu, M. M., Xavier, R. J., Demay, M. B., Russell, R. G., Factor, S. et al. (2001). TBX1 is responsible for cardiovascular defects in velo-cardio-facial/DiGeorge syndrome. *Cell* **104**, 619-629.

Meyers, E. N. and Martin, G. R. (1999). Differences in left-right axis pathways in mouse and chick: functions of FGF8 and SHH. *Science* **285**, 403-406.

Moon, A. M. and Capecchi, M. R. (2000). Fgf8 is required for outgrowth and patterning of the limbs. *Nat. Genet.* **26**, 455-459.

Nagy, A., Rossant, J., Nagy, R., Abramow-Newerly, W. and Roder, J. C. (1993). Derivation of completely cell culture-derived mice from early-passage embryonic stem cells. *Proc. Natl. Acad. Sci. USA* **90**, 8424-8428.

Oelgeschlager, M., Larrain, J., Geissert, D. and de Robertis, E. M. (2000). The evolutionarily conserved BMP-binding protein Twisted gastrulation promotes BMP signalling. *Nature* **405**, 757-763.

Oelgeschlager, M., Kuroda, H., Reversade, B. and de Robertis, E. M. (2003). Chordin is required for the Spemann organizer transplantation phenomenon in Xenopus embryos. *Dev. Cell* **4**, 219-230.

Oster, G., Kilburn, K. H. and Siegal, F. P. (1983). Chemically induced congenital thymic dysgenesis in the rat: a model of the DiGeorge syndrome. *Clin. Immunol. Immunopathol.* **28**, 128-134.

Papaioannou, V. E. and Silver, L. M. (1998). The T-box gene family. *BioEssays* **20**, 9-19.

Pappano, W. N., Scott, I. C., Clark, T. G., Eddy, R. L., Shows, T. B. and Greenspan, D. S. (1998). Coding sequence and expression patterns of mouse chordin and mapping of the cognate mouse chrd and human CHRD genes. *Genomics* **52**, 236-239.

Peters, H. and Balling, R. (1999). Teeth. Where and how to make them. *Trends Genet.* **15**, 59-65.

Peters, H., Neubuser, A., Kratochwil, K. and Balling, R. (1998). Pax9-deficient mice lack pharyngeal pouch derivatives and teeth and exhibit craniofacial and limb abnormalities. *Genes Dev.* **12**, 2735-2747.

Piccolo, S., Agius, E., Lu, B., Goodman, S., Dale, L. and de Robertis, E. M. (1997). Cleavage of Chordin by Xolloid metalloprotease suggests a role for proteolytic processing in the regulation of Spemann organizer activity. *Cell* **91**, 407-416.

Pingault, V., Bondurand, N., Kuhlbrodt, K., Goerich, D. E., Prehu, M. O., Puliti, A., Herbarth, B., Hermans-Borgmeyer, I., Legius, E., Matthijs, G. et al. (1998). SOX10 mutations in patients with Waardenburg-Hirschsprung disease. *Nat. Genet.* **18**, 171-173.

Piotrowski, T. and Nusslein-Volhard, C. (2000). The endoderm plays an important role in patterning the segmented pharyngeal region in zebrafish (Danio rerio). *Dev. Biol.* **225**, 339-356.

Raff, R. A. (1996). *The Shape of Life*. Chicago, IL: University of Chicago Press.

Rodriguez-Esteban, C., Tsukui, T., Yonei, S., Magallon, J., Tamura, K. and Izpisua Belmonte, J. C. (1999). The T-box genes Tbx4 and Tbx5 regulate limb outgrowth and identity. *Nature* **398**, 814-818.

Ryan, A. K., Goodship, J. A., Wilson, D. I., Philip, N., Levy, A., Seidel, H., Schuffenhauer, S., Oechsler, H., Belohradsky, B., Prieur, M. et al. (1997). Spectrum of clinical features associated with interstitial chromosome 22q11 deletions: a European collaborative study. *J. Med. Genet.* **34**, 798-804.

Sasai, Y., Lu, B., Steinbeisser, H., Geissert, D., Gont, L. K. and de Robertis, E. M. (1994). Xenopus chordin: a novel dorsalizing factor activated by organizer-specific homeobox genes. *Cell* **79**, 779-790.

Schulte-Merker, S., Lee, K. J., McMahon, A. P. and Hammerschmidt, M. (1997). The zebrafish organizer requires chordino. *Nature* **387**, 862-863.

Slack, J. M., Holland, P. W. and Graham, C. F. (1993). The zootype and the phylotypic stage. *Nature* **361**, 490-492.

Solloway, M. J. and Robertson, E. J. (1999). Early embryonic lethality in Bmp5;Bmp7 double mutant mice suggests functional redundancy within the 60A subgroup. *Development* **126**, 1753-1768.

Strachan, T. and Read, A. P. (1994). PAX genes. *Curr Opin Genet Dev* **4**, 427-438.

Sun, X., Meyers, E. N., Lewandoski, M. and Martin, G. R. (1999). Targeted disruption of Fgf8 causes failure of cell migration in the gastrulating mouse embryo. *Genes Dev.* **13**, 1834-1846.

Taddei, I., Morishima, M., Huynh, T. and Lindsay, E. A. (2001). Genetic factors are major determinants of phenotypic variability in a mouse model of the DiGeorge/del22q11 syndromes. *Proc. Natl. Acad. Sci. USA* **98**, 11428-11431.

Tassabehji, M., Newton, V. E. and Read, A. P. (1994). Waardenburg syndrome type 2 caused by mutations in the human microphthalmia (MITF) gene. *Nat. Genet.* **8**, 251-215.

Trumpp, A., Depew, M. J., Rubenstein, J. L., Bishop, J. M. and Martin, G. R. (1999). Cre-mediated gene inactivation demonstrates that FGF8 is required for cell survival and patterning of the first branchial arch. *Genes Dev.* **13**, 3136-3148.

Vitelli, F., Morishima, M., Taddei, I., Lindsay, E. A. and Baldini, A. (2002a). Tbx1 mutation causes multiple cardiovascular defects and disrupts neural crest and cranial nerve migratory pathways. *Hum. Mol. Genet.* **11**, 915-922.

Vitelli, F., Taddei, I., Morishima, M., Meyers, E. N., Lindsay, E. A. and Baldini, A. (2002b). A genetic link between Tbx1 and fibroblast growth factor signaling. *Development* **129**, 4605-4611.

Wendling, O., Dennefeld, C., Chambon, P. and Mark, M. (2000). Retinoid signaling is essential for patterning the endoderm of the third and fourth pharyngeal arches. *Development* **127**, 1553-1562.

Wilson, D. I., Cross, I. E., Wren, C., Scambler, P. J., Burn, J. and Goodship, J. A. (1994). Minimum prevalence of 22q11 deletions. *Am. J. Hum. Genet. (suppl.)* **55**, A975.

Yamada, M., Revelli, J. P., Eichele, G., Barron, M. and Schwartz, R. J. (2000). Expression of chick Tbx-2, Tbx-3, and Tbx-5 genes during early heart development: evidence for BMP2 induction of Tbx2. *Dev. Biol.* **228**, 95-105.

Zhang, H. and Bradley, A. (1996). Mice deficient for BMP2 are nonviable and have defects in amnion/chorion and cardiac development. *Development* **122**, 2977-2986.